High-speed two-dimensional phased-array antenna scanning using acousto-optics

Riza, Nabeel

Nabeel A. Riza, "High-speed two-dimensional phased-array antenna scanning using acousto-optics," Proc. SPIE 1703, Optical Technology for Microwave Applications VI and Optoelectronic Signal Processing for Phased-Array Antennas III, (2 December 1992); doi: 10.1117/12.138415

SPIE.

Event: Aerospace Sensing, 1992, Orlando, FL, United States

HIGH SPEED TWO DIMENSIONAL PHASED ARRAY ANTENNA SCANNING USING ACOUSTO-OPTICS

Nabeel A. Riza

General Electric Corporate Research and Development
P. O. Box 8, KWB 617
Schenectady, N.Y. 12301

ABSTRACT

A novel in-line additive acousto-optic architecture for planar phased arrays is described for two dimensional beam scanning. A concept acousto-optic processor is demonstrated in the laboratory, and the required modulo-2π phase control is achieved using two control signals. Up-to K_u band operation is possible with this processor.

2. INTRODUCTION

Recently, we introduced and experimentally demonstrated an in-line additive acousto-optic (AO) architecture for controlling phase-based phased array antennas [1-4]. This system provided rapid antenna beam scanning capability along one direction. Most high performance phased arrays are planar arrays that require modulo-2π phase-based control for two dimensional (2-D) antenna scanning. In this paper, we describe a novel in-line additive AO architecture that can provide the desired high speed (0.4 μsec) phase-based antenna scanning along two independent antenna beam directions [5]. This processor uses AO devices in a crossed Bragg cell configuration. 2-D beam position is controlled via two independent analog control signals, and the phase and carrier can be independently set to a desired value. Experimental results are described, and system issues are discussed.

3. TWO DIMENSIONAL BEAM SCANNING THEORY

For a planar array with a typical rectangular grid placing of the antenna elements (see Fig.1), it is possible to steer the antenna pencil beam independently in azimuth as well as height directions by simply controlling the phase of the signals driving the elements in the 2-D array. As shown in Fig.1, the beam position in a spherical coordinate geometry is given by the coordinates θ and ϕ, that define a point on a unit hemisphere. Here, θ is the angle of scan measured from the broadside direction, and ϕ is the plane of scan measured from the x' axis, where (x',y') are the beam space cartesian coordinates. Von Aulock [6] proposed a simplified method for describing the beam 2-D position in terms of direction cosines, where the projection of the point on the unit hemisphere on a plane defines the beam coordinates. Here, the plane axes, in terms of any beam direction θ and ϕ, are given by the direction cosines

$$\cos(\alpha_{x'})=\sin(\theta)\cos(\phi), \quad \cos(\alpha_{y'})=\sin(\theta)\sin(\phi). \qquad (1)$$

For a particular desired beam position corresponding to the direction cosines $\cos(\alpha_{x'S})$ and $\cos(\alpha_{y'S})$ for a linear phase taper, the signal feeding the mn^{th} element in the antenna array located at $(mD_{x'}, nD_{y'})$ is given by [6]

$$i_{mn}(t)= A_{mn}\cos[\omega_r t + m\,\phi_{x'} + n\,\phi_{y'}), \qquad (2)$$

where A_{mn} is the signal amplitude, ω_r is the antenna carrier frequency, and $\phi_{x'}$ and $\phi_{y'}$ are the element to element phase shifts along the x' and y' directions, respectively. The phase shifts are given by the expressions

$$\phi_{x'} =(2\pi/\lambda_r)D_{x'}\cos(\alpha_{x'S}), \qquad \phi_{y'} =(2\pi/\lambda_r)D_{y'}\cos(\alpha_{y'S}), \qquad (3)$$

 0-8194-0868-9/92/$4.00

where, $D_{x'}$ and $D_{y'}$ are the antenna inter-element spacings along the x' and y' directions, respectively, and the beam position given in a spherical coordinate geometry is

$$\phi_S=\tan^{-1}[\cos(\alpha_{y'S})/\cos(\alpha_{x'S})]\,, \qquad \theta_S=\sin^{-1}[\cos(\alpha_{x'S})/\cos(\phi_S)]. \qquad (4)$$

Here, λ_r is the antenna carrier wavelength, θ_S is the angle of scan measured from the broadside direction, and ϕ_S is the plane of scan measured from the x' axis.

4. THE AO SYSTEM FOR 2-D PHASED ARRAY ANTENNA CONTROL

Fig.2 shows the AO system that can generate the appropriate phase signals represented by Eqn.2, for providing 2-D beam steering in a planar phased array antenna. Here, independent antenna beam height and azimuth control for a planar phased array can be achieved by using four 1-D AO devices (AODs)/Bragg cells in a crossed cell, in-line additive configuration. This processor consists of a high power laser source, four AOD's, a 2-D high speed fiber/detector array, imaging and Fourier transforming optics, and three signal generators to provide the antenna carrier and azimuth/height control signals. The microwave signals feeding the different AODs are

$$\begin{aligned} s_{aod\,1} &= a\cos(\omega_c+\omega_1)t \quad , s_{aod\,4} = a\cos(\omega_c-\omega_1)t \quad , \\ s_{aod\,2} &= a\cos(\omega_c-\omega_2)t \quad , s_{aod\,3} = a\cos(\omega_c+\omega_2)t. \end{aligned} \qquad (5)$$

Here `a' is the amplitude of the signals, ω_c is the microwave frequency (within the AOD bandwidth centered around the AOD center frequency), and ω_1 and ω_2 are the radio frequency (rf) antenna scan control frequencies. The signals in Eqn.5 can be generated by separately mixing the rf control signals with the microwave carrier of frequency ω_c. The mixing operation generates an amplitude modulated signal with upper and lower sidebands, that, after appropriate electronic/optical filtering, give the desired drive single-sideband (SSB) signal for a particular AOD. ω_1 and ω_2 are the independent beam scan control parameters for positioning the antenna pencil beam at the desired coordinates θ_S, ϕ_S, given in a spherical geometry.

The AO system's top and side views are shown in Fig.3, and the system works as follows. Light from a laser/laser diode, collimated along the x direction, and focussed along the y direction by a cylindrical lens C1, is incident at Bragg angle along the acoustic column of AOD1. The DC (undiffracted) and +1 order (diffracted) beams from AOD1 are spatially separated by the spherical lens S1, forming two separate vertical slits of light. The orthogonally oriented (along y direction) AOD2 and AOD3 Bragg cells are positioned such that the DC and +1 order slits from AOD1 fall within AOD2 and AOD3 acoustic columns, respectively. AOD2 is Bragg matched such that the DC light from AOD1 generates a -1 order from AOD2. The undiffracted light from AOD2 is blocked in the plane of AOD4. Similarly, AOD3 is Bragg matched such that the +1 order from AOD1 generates a +1 order from AOD3. The undiffracted light from AOD3 is blocked in the plane of AOD4. The spherical lens S2 focuses the diffracted and undiffracted orders from AOD2 and AOD3 into vertically separated horizontal slits. The acoustic column of AOD4 is placed such that it encloses the horizontal slit from the diffracted orders from AOD2 and AOD3. The other horizontal slit from the undiffracted light from AOD2 and AOD3 is blocked. The -1 order from AOD2 is used to generate a -1 order from AOD4, while the +1 order from AOD3 passes essentially uneffected through AOD4. The two beams, that is the DC beam through AOD4 (which is also the +1 order from AOD3), and the -1 order from AOD4, are interfered on a 2-D fiber/detector array, that in-turn generates the necessary signals for 2-D beam steering for a planar phased array. After an M_X and M_Y times magnification along the x and y directions, respectively, using the imaging systems shown in Fig.3, the current generated from the mn^{th} fiber/detector pair in the sampling 2-D array can be approximated as [5]

$$i_{mn}(t) = G\cos\left[\omega_r t - m\psi_x - n\psi_y\right], \qquad (6)$$

where the antenna carrier angular frequency is given by $\omega_r=4\omega_c$, and the phase difference between the signals driving the antennas along the x' and y' directions, are given by

$$\psi_x = \frac{2\omega_1 l_x}{M_x v_a} \quad , \quad \psi_y = \frac{2\omega_2 l_y}{M_y v_a} . \tag{7}$$

where l_x and l_y are the inter-fiber spacings along the x and y directions, respectively, the bias term has been dropped, G is a constant term, and m=0,1,2,.....,M; n=0,1,2,....,N. Here M and N are the total number of fibers/detectors along the x and y directions, respectively. Because the inter-fiber spacing is fixed, the 2-D fiber array performs linear phase sampling along the x and y directions. This linear phase sampling forms the basis of generating the M X N appropriately phased signals for independently steering a M X N element planar phased array along the height and azimuth directions. Note that $4\omega_c$ forms the antenna carrier, while ω_1 independently controls the antenna beam scanning in one direction, and ω_2 controls the beam scanning in the other (orthogonal) direction. Comparing equations 2 and 6, the 2-D beam steering conditions for the optical processor for positioning the antenna beam at the direction cosines $\cos(\alpha_{x's})$ and $\cos(\alpha_{y's})$ are given by

$$\psi_x = \phi_{x's} + p2\pi = 2\pi\left(D_{x's} / \lambda_r\right)\cos(\alpha_{x's}) + p2\pi \ ,$$
$$\psi_y = \phi_{y's} + q2\pi = 2\pi\left(D_{y's} / \lambda_r\right)\cos(\alpha_{y's}) + q2\pi \ , \tag{8}$$

where p,q=0,±1,±2,..... .

5. EXPERIMENTAL DEMONSTRATION OF THE AO SYSTEM

The AO system shown in Figures 2 and 3 is set-up on an optical bench (without air floatation) in the laboratory. The high power laser source is a 514 nm, 200 mW output power Ar+ ion laser. The light is spatially filtered using a 25 μm pin-hole , 10 X microscope assembly. The filtered laser light is collimated by a 15 cm focal length (FL) spherical lens S, forming a 22 mm diameter collimated optical beam. This collimated beam is focussed into AOD1 using a 30 cm FL cylindrical lens C1. All the AODs used in the system are flint glass devices with a 70 MHz center frequency, 40 MHz bandwidth, and 10 μsec time-aperture. Spheres S1 and S2 with 50 cm focal lengths form a 1 : 1 imaging system between the AOD1 and AOD4 planes. The large 50 cm FL of S1 is used to ensure that the diffracted (+1 order) and undiffracted (DC) beams from AOD1 have adequate spatial separation in the front focal plane of lens S1, in order that the undiffracted beam is positioned within the acoustic column of AOD2, and the diffracted beam is positioned in AOD3. The large separation between the DC and +1 order beams from AOD1 is required as the flint glass AODs have a large (4 mm) acoustic beam height dimensions (or cell thickness), preventing AOD2 and AOD3 to be positioned very close (e.g. 0.2 mm) apart. The DC light beams from AOD2 and AOD3 are blocked by the metallic casing of AOD4, which acts as a DC block. The undiffracted light beam from AOD4 is blocked in the front Fourier plane of cylindrical lens C2 with FL=20 cm. The cylindrical lens C3 of FL=30 cm and the sphere S2 of FL=50 cm form an imaging system along the y-direction with a magnification M_y=30/50=0.6. Here, the AOD2/AOD3 plane is imaged along the y-direction on to the processor output plane where the 2-D fiber array is positioned. The 10 cm FL cylinder C4 and the cylinder C2 form an imaging system along the x-direction with a magnification M_x=10/20=0.5. Here, AOD4 plane is imaged along the x-direction on-to the processor output plane.

For concept demonstration, the 2-D fiber/detector array is simulated by two avalanche photodiodes (APDs) that are placed with inter-detector spacings of l_x= 6 mm and l_y= 5.6 mm. The APDs are Hamamatsu model S2381 operated with 159 V bias. AOD1 and AOD4 are driven by 20.3 Vp-p at 50 ohm 90 MHz rf signals, while AOD2 and AOD3 are driven by 22.7 Vp-p at 50 ohm, 75 MHz rf signals. The measured AOD diffraction efficiency for all the Bragg cells is approximately 10 %. All the signals driving the AODs are mutually phase coherent as all signal generators used in the experiment are externally locked to a stable 10 MHz reference oscillator. The two multiple-diffracted beams generated from the AODs are incident at the APD plane. The APDs implement the optical heterodyning operation, generating 330 MHz rf signals, as a summation of the signal frequencies driving the AODs is 330 MHz, i.e. 75 +75 + 90 + 90 = 330 MHz. The 330 MHz signal directly measured from one of the APDs is shown in Fig.4. This signal showed a dynamic range of 48 dB at 1 MHz, a carrier-to-noise ratio of 109.9 dB/Hz at 1 MHz, and an output power level of -19.1 dBm (see Figures 5-7).

The 2-D modulo-2π phase control experiment is performed as follows. First, phase control along the x-direction of the processor is measured using the pair of APDs with an inter-detector spacing along x-direction of l_x=6 mm. In this case, the frequency of the signals driving AOD2 and AOD3 is kept fixed at 75 MHz. On the otherhand, AOD1 and AOD4 are driven by upper and lower sideband signals, respectively. The SSB signals are generated from two phase-locked signal generators. Here AOD1 is driven by a signal with frequency 90 MHz + f_1 KHz, and AOD2 is driven by a signal with frequency 90 MHz - f_1 KHz. f_1 controls the relative phase shift of the 330 MHz rf output signals, providing 1-D scan control (e.g., in azimuth) for the radar beam. Fig.8 shows the oscilloscope traces of the 330 MHz signals, with changing relative phase-shift. The upper trace is from one APD, while the lower oscilloscope trace is from the other APD. Fig.9 shows the measured phase shift behavior with changing control frequency f_1. The measurements show the expected linear phase control. A 2π phase shift is obtained for f_1=170 KHz.

Phase control along the y-direction of the processor is measured in a similar fashion. In this case, the signals feeding AOD1 and AOD4 have a fixed frequency of 90 MHz, while AOD2 and AOD3 are fed by SSB signals centered at 75 MHz. AOD2 is fed by a lower sideband signal of frequency 75 MHz - f_2 KHz, and AOD3 is fed by an upper sideband signal of frequency 75 MHz + f_2 KHz. Here, f_2 controls the relative phase shift between the 330 MHz output signals generated by the APD pair having a inter-detector spacing l_y=5.6 mm along the y-direction. These 330 MHz output signals provide 1-D scan control along the orthogonal (e.g., elevation) beam scan direction of the radar. Fig.10 shows the measured phase shift behavior with changing control frequency f_2. The measurements show the expected linear phase control. A 2π phase shift is obtained for f_2=210 KHz.

Because the proposed processor can control phase shift along two independent directions, that is, the x and y directions of the processor, using the two independent control parameters f_1 an f_2, it is possible to generate signals with the desired phase-shifts necessary for steering a planar phased-array antenna beam in 2-D space. The experiment demonstrated signal phase control behavior along the two independent directions (x and y) of the processor, first by varying f_1, and then by varying f_2. Thus, if f1 and f2 are independently and simultaneously varied for the processor, it is possible to get 2-D antenna beam steering.

6. SYSTEM ISSUES

Output signal phase stability is a very important requirement for radar applications. Fig.11 shows the analog oscilloscope traces for the APD pair outputs, indicating high relative phase shift stability. Fig.12 shows the 330 MHz APD signal output relative to the 75 MHz signal driving AOD2 and AOD3. This photograph also shows the processor output signal phase stability. Note that because the processor has an almost common-path in-line additive interferometric design, it forms a very stable interferometer. This concept processor used rf Bragg cells that required rather long focal length lenses to implement the design. Nevertheless, the long length (> 3 m) of the processor did not prevent the output from having good signal phase stability.

An important feature of this processor is its wide carrier tunable bandwidth. By varying the frequency of the signals driving the AOD pairs, that is, AOD1/AOD4 pair, and AOD2/AOD3 pair, it is possible to vary the APD output signal frequency. For the concept processor, the output signal showed a frequency variation from 280 MHz to 370 MHz, showing a 90 MHz tunable bandwidth (see Fig.13 and Fig.14).

There are various configurations of the AO system based on whether rf or GHz band Bragg cell pairs are used for the AOD1/AOD4 and AOD2/AOD3 pairs. One key diiference between the rf and GHz band cells is the acoustic height dimensions H. As an example, for rf cells, H = 4 mm, while for GHz cells, H=0.4 mm. This means that if GHz cells are used for AOD2/AOD3, the cells can be positioned very close, preventing the use of long FL lenses, as used in the concept processor with rf cells. GHz cells can also be used for AOD1/AOD4 cells. In the concept processor, rf cells were used for AOD1/AOD4. This resulted in a much smaller spatial separation between the +1 and DC beams from AOD1; thus a long focal length lens was used as the Fourier transform lens. Thus, by using GHz cells for AOD1/AOD4, the processor can be made much smaller. To maintain a wide tunable bandwidth, either rf cells (having large H's) can be used for AOD2/AOD3 pair, or multiple channel GHz band cells can be used for AOD3, with AOD2 being a single channel GHz cell.

Because this processor uses 4 Bragg cells that are low diffraction efficiency optical devices, it is imperative that a high power (e.g., 2 W) laser source and high gain (e.g., 80) APDs be employed in the processor. Because of optical efficiency

constraints, this processor is suited for controlling medium sized (i.e., 1000 elements or less) planar phased-arrays that require extremely fast (e.g., 400 nsec) beam switching speeds that may be required for tracking multiple fast moving targets. Moreover, phase control for the system is achieved with only two control signals, thus drastically reducing control hardware requirements. The processor can be engineered to a compact, robust system.

7. CONCLUSION

This paper has introduced and experimentally demonstrated a phase-based acousto-optic technique for control and signal processing in planar phased array antennas. The system provides 2-D antenna scanning using two analog control signals. The optical control system is suitable for medium size (e.g., < 1000 elements), very high beam switching speed (e.g., 400 nsec), planar phased-arrays used in compact, mobile scenarios, such as airborne or space-based applications, or small ground-based units.

8. ACKNOWLEDGEMENTS

Support from the GECRD and GE-Aerospace is greatly acknowledged.

9. REFERENCES

[1] N. A. Riza, ``Novel acousto-optic systems for spectrum analysis and phased array radar signal processing," Chapter 6, Ph.D Thesis, Caltech, Oct., 1989.

[2] N. A. Riza and D. Psaltis, ``Acousto-optic signal processors for transmission and reception of phased array antenna signals," *Journal of Applied Optics*, vol.30, no.23, pp.3294-3303, 1991.

[3] N. A. Riza, ``Acousto-optic techniques for phased array antenna processing," *Proc. SPIE Conf. Emerging Optoelec. Tech.* , vol. 1622, No.21, Dec., 1991.

[4] N. A. Riza, ``An acousto-optic phased array antenna beamformer with independent phase and carrier control using single sideband signals," *IEEE Photonics Tech. Lett.*, Vol.4, No.2, February, 1992.

[5] N. A. Riza, ``Acousto-optic architecture for two dimensional beam scanning in phased array antennas," to appear in *Journal of Applied Optics*, Vol.31, 1992.

[6] W. H. Von Aulock, `` Properties of Phased Arrays," *IRE Trans.*, Vol. AP-9, pp. 1715-1727, 1960.

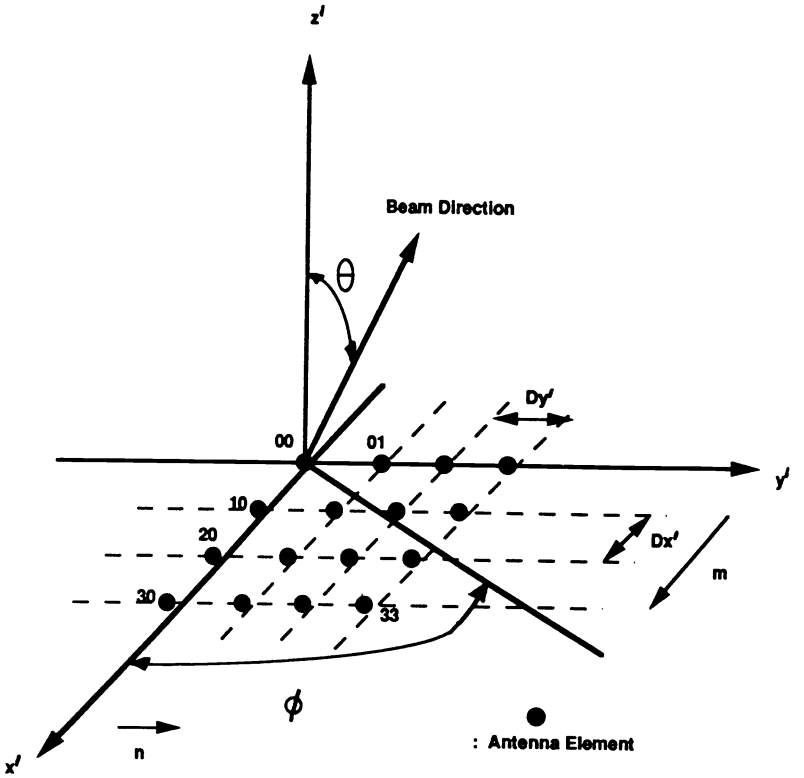

Fig.1 Planar phased array element rectangular grid geometry and beam scanning notation.

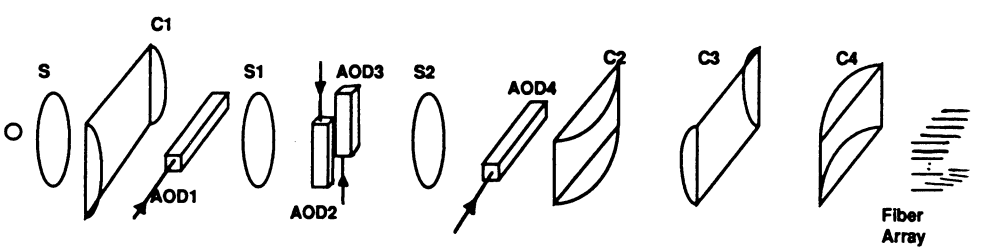

Fig.2 AO architecture for 2-D scan control of planar phased arrays.

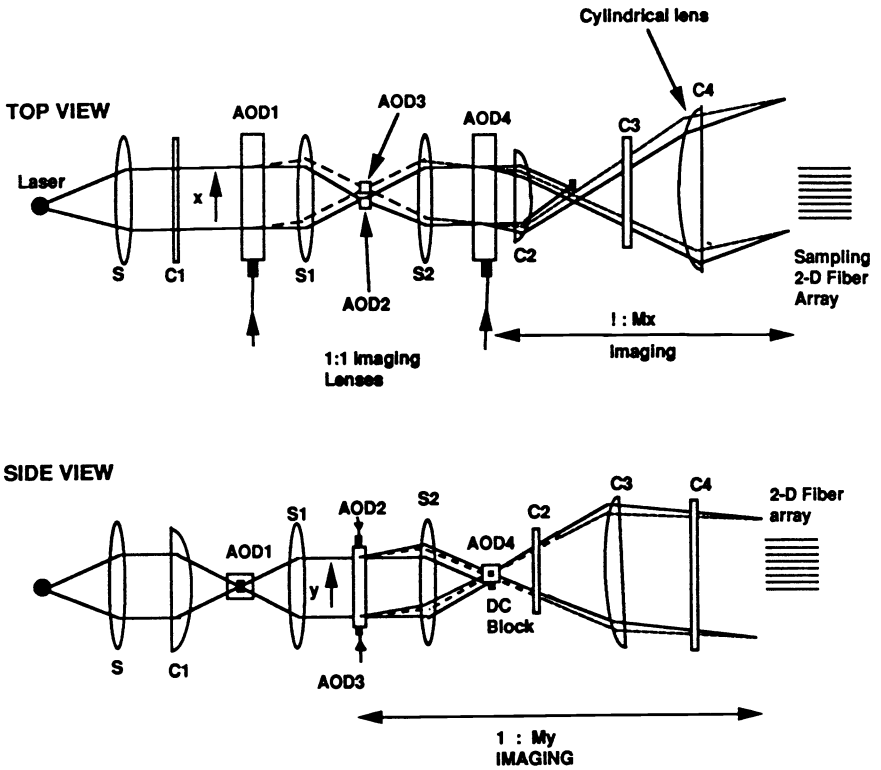

Fig.3 Top and side views of the AO architecture.

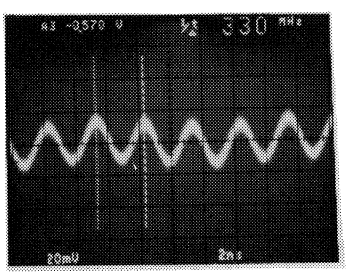

Fig.4 The 330 MHz signal directly measured from one of the APDs.

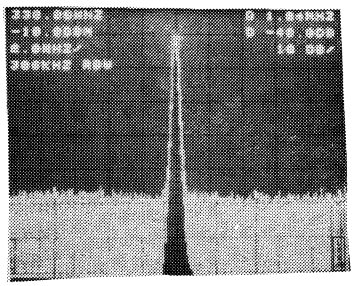

Fig.5 The 330 MHz signal showed a dynamic range of 48 dB at 1 MHz.

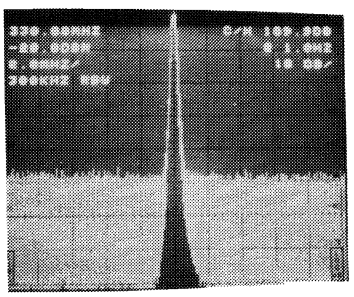

Fig.6 The 330 MHz signal showed a carrier-to-noise ratio of 109.9 dB/Hz at 1 MHz.

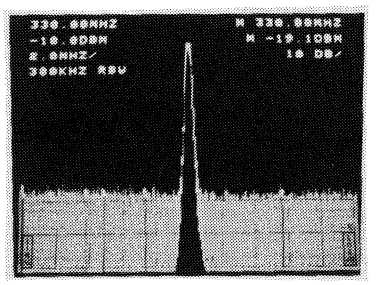

Fig.7 The 330 MHz signal showed an output power level of -19.1 dBm.

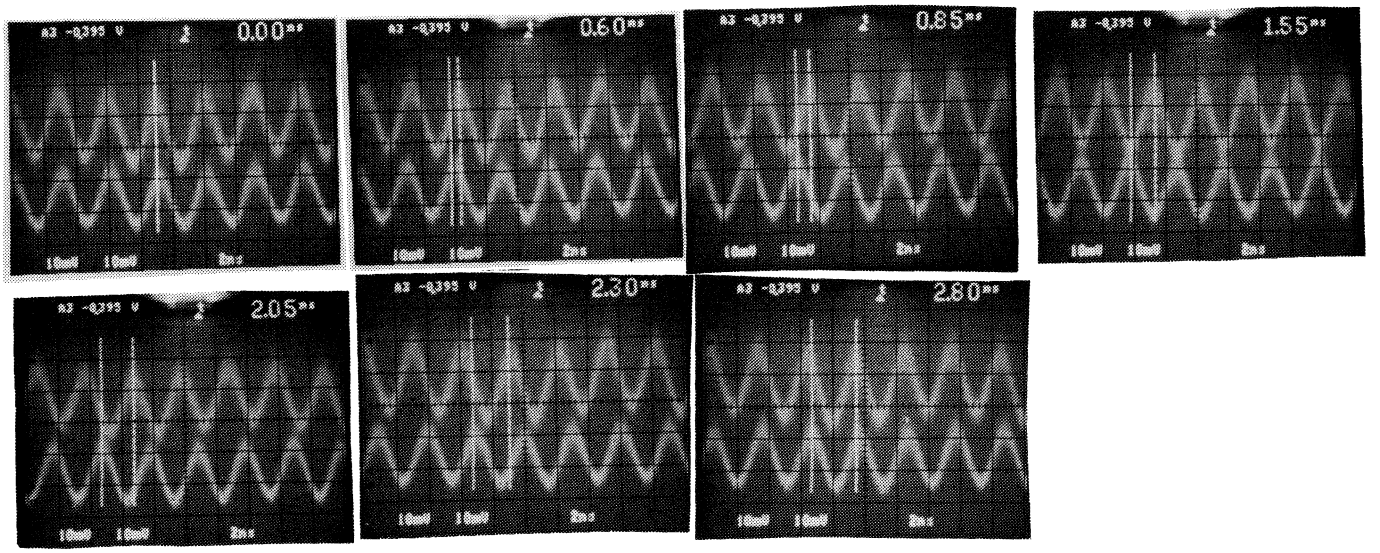

Fig.8 shows the oscilloscope traces of the 330 MHz signals, with changing relative phase-shift. The upper trace is from one APD, while the lower oscilloscope trace is from the other APD.

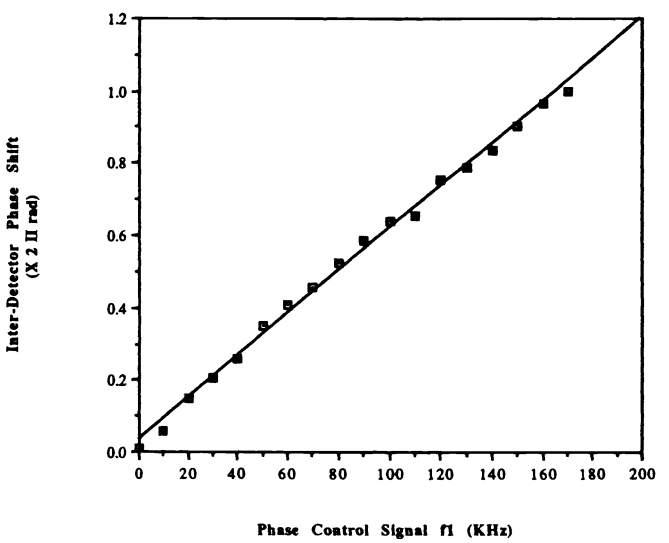

Fig.9 shows the measured phase shift behavior with changing control frequency f_1. A 2π phase shift is obtained for f_1=170 KHz.

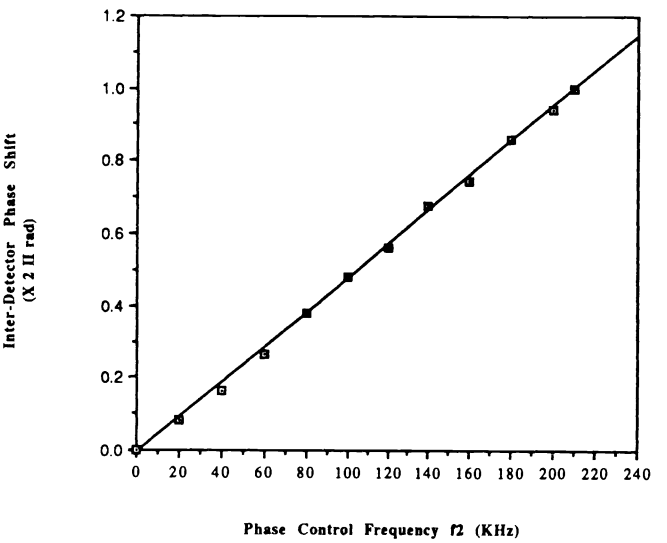

Fig.10 shows the measured phase shift behavior with changing control frequency f_2. A 2π phase shift is obtained for f_2=210 KHz.

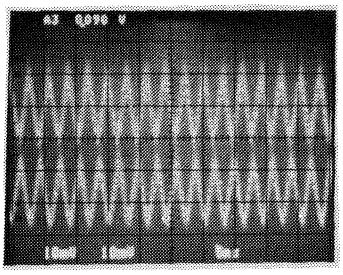

Fig.11 shows the analog oscilloscope traces for the APD pair outputs, indicating high relative phase shift stability.

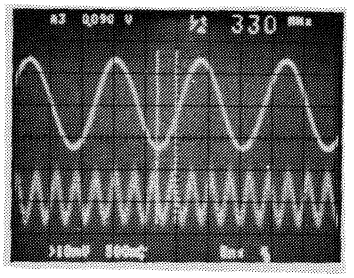

Fig.12 shows the 330 MHz APD signal output relative to the 75 MHz signal driving AOD2 and AOD3. This photograph also shows the processor output signal phase stability.

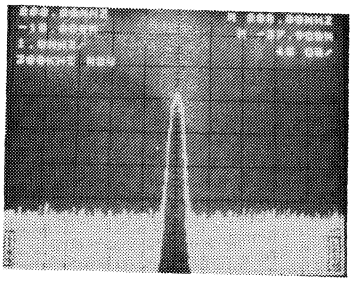

Fig.13 shows a 280 MHz output signal for the concept processor.

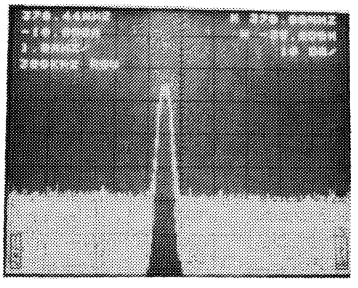

Fig.14 shows a 370 MHz output signal for the concept processor, showing (with Fig.13) a 90 MHz carrier tunable bandwidth.